Shape effects in the fluctuations of random isochrones on a square lattice

Iván Álvarez Domenech [1,*], Javier Rodríguez-Laguna [2], Rodolfo Cuerno [3], Pedro Córdoba-Torres [1],
and Silvia N. Santalla [4]

[1]*Dto. Física Matemática y de Fluidos, Universidad Nacional de Educación a Distancia, Las Rozas 28232, Spain*
[2]*Dto. Física Fundamental, Universidad Nacional de Educación a Distancia, Madrid 28040, Spain*
[3]*Dto. Matemáticas & GISC, Universidad Carlos III de Madrid, Leganés 28911, Spain*
[4]*Dto. Física & GISC, Universidad Carlos III de Madrid, Leganés 28911, Spain*

We consider the isochrone curves in first-passage percolation on a 2D square lattice, i.e., the boundary of the set of points which can be reached in less than a given time from a certain origin. The occurrence of an instantaneous average shape is described in terms of its Fourier components, highlighting a crossover between a diamond and a circular geometry as the noise level is increased. Generally, these isochrones can be understood as fluctuating interfaces with an inhomogeneous local width which reveals the underlying lattice structure. We show that once these inhomogeneities have been taken into account, the fluctuations fall into the Kardar-Parisi-Zhang universality class with very good accuracy, where they reproduce the Family-Vicsek Ansatz with the expected exponents and the Tracy-Widom histogram for the local radial fluctuations.

I. INTRODUCTION

Random curves have attracted attention in many fields of science [1], such as physics, mathematics, and biology. For instance, they appear in fields such as polymer physics [2], quantum gravity [3], or the characterization of biophysical objects such as membranes and cells [4]. Let us focus on isochrone curves within a random two-dimensional manifold, i.e., the boundaries of balls with different radii, when the metric is flat on average and presents only short-range correlations. It was shown in previous work [5,6] that in the continuum these isochrones present a fractal behavior described by the celebrated Kardar-Parisi-Zhang (KPZ) universality class, which accounts for the fluctuation statistics of many growing interfaces [7–9]. The average roughness of the isochrone, $W(t)$, defined as the root-mean-square deviation of the ball radii at time t, grows as $W(t) \sim t^\beta$, while the correlation length ξ grows as $\xi \sim t^{1/z}$, where $\beta = 1/3$ and $z = 3/2$ are, respectively, the growth exponent and the dynamic exponent for the 1+1 dimensional (1+1D) KPZ universality class. Moreover, for long times, the local roughness at a length scale l behaves as $w(l) \sim l^\alpha$, where α is called the roughness exponent, which is related to the other two through the Family-Vicsek relation $\alpha = \beta z$, and takes the value $1/2$ for the KPZ class.

The discrete analog of this problem is known as first-passage percolation (FPP) [10], which was originally proposed as a model of fluid flow through random media. The FPP model has received substantial attention within probability theory, giving rise to important results such as the

subadditive ergodic theorem [11], which has remarkable relevance for classical problems such as the Ulam-Hammersley problem, and contributed to develop the field of integrable probability [12]. Moreover, integrable probability was, in turn, instrumental to characterize the one-point and two-point fluctuations within the KPZ universality class, specifically the emergence of the Tracy-Widom (TW) distributions [13–15], which were originally defined as the probability distributions for extreme eigenvalues in random matrix ensembles [16]. The FPP model has been thoroughly studied numerically in our previous work [17,18], both in the weak and strong disorder regimes, confirming the predictions regarding KPZ scaling in the asymptotic regime for the geodesics. Yet, a similar characterization of the statistical properties of the isochrones has not been reported so far, to the best of our knowledge, which is the task undertaken in this paper. The main difficulty to this end is the fact that the average shape of the isochrones is not circular, in general, due to the anisotropy of the lattice. In fact, the existence and characterization of such average shapes in the long run constitute a relevant area of mathematical research, which has led to the celebrated shape theorem [19,20].

More generally, many other contexts for the growth of planar clusters present analogous complexities, in the sense that nontrivial interface fluctuations occur around well-defined macroscopic shapes. Examples can be found, for instance, in different growth processes on a lattice [21], in epitaxial growth of thin solid films in the submonolayer regime [22], or in the spreading of precursor layers of wetting fluids [23–25]. Both of these systems inherently host strong interface fluctuations due to the small typical scales which are involved. And also, in both cases, being able to subtract characteristic shapes from front fluctuations can prove significant to correctly identify the universality class (if appropriate) of the latter.

*iadomenech@dfmf.uned.es

034104-1

This paper is organized as follows. We start with a description of the basic properties of the FPP model in Sec. II. In Sec. III, we characterize the instantaneous average shape (IAS) of the isochrones for different noise levels using their Fourier components. The growth and dynamic exponents, β and z, are determined in Sec. IV, and the histogram of the radial fluctuations is obtained in Sec. V. In both cases, the lattice anisotropy masks the expected KPZ behavior unless the statistical data are angularly resolved. The roughness exponent, α, presents an additional numerical challenge because any uncertainty in the IAS may interfere with its measurement. In Sec. VI, we address this issue, and we find that the aforementioned uncertainty manifests itself as an intrinsic roughness. The paper concludes in Sec. VII with a discussion of our main conclusions and suggestions for further work.

II. MODEL

Let us consider the integer lattice $\mathbb{Z}^2$, with edge set E. We can associate a random variable $\tau_e > 0$ to each edge $e \in E$, which we will call its passage time or link time. The variables $\{\tau_e\}_{e \in E}$ are assumed to be independent, identically distributed (i.i.d.), with distribution function $F(\tau)$, such that $F(0) = 0$, i.e., we assume that τ_e is strictly positive with probability one. The associated density function will be denoted by $f(\tau)$, and μ and s will denote, respectively, its mean and deviation, which we will assume to be finite.

A finite path is defined as a sequence of edges, $e_1, e_2, \ldots, e_n$, such that e_i and e_{i+1} share exactly one endpoint. For each path $\gamma = \{e_1, \ldots, e_n\}$, we can define its passage time $T(\gamma)$ as $T(\gamma) = \sum_i \tau_i$, where the sum runs over all edges in γ. Finally, given two different nodes, $\mathbf{x}, \mathbf{y} \in \mathbb{Z}^2$, we can define the passage time between them, $T(\mathbf{x}, \mathbf{y})$, as the minimum passage time over all paths joining $\mathbf{x}$ with $\mathbf{y}$, which we will denote by

$$T(\mathbf{x}, \mathbf{y}) = \min_{\gamma \in \Gamma(\mathbf{x}, \mathbf{y})} T(\gamma), \qquad (1)$$

where $\Gamma(\mathbf{x}, \mathbf{y})$ denotes the set of paths joining these two points. The random function $T(\mathbf{x}, \mathbf{y})$ plays the role of a distance, and the pair $(\mathbb{Z}^2, T(\cdot, \cdot))$ defines a metric space in which the geodesic between two nodes is given by the path of minimal arrival time [17]. The FPP model is mathematically equivalent to the problem of optimal paths in weighted networks [26,27]. Depending on the properties of the network and on the physical meaning of the weights assigned to the links, we may find a wide variety of applications. For example, for directed lattices and bond weights representing the local energy, we get the problem of directed polymers in random media [2,28].

We can define the ball $B(t; \mathbf{x}_0)$ around a fixed node $\mathbf{x}_0$ for time $t \geqslant 0$,

$$B(t; \mathbf{x}_0) = \{\mathbf{x} \in \mathbb{Z}^2 \,:\, T(\mathbf{x}_0, \mathbf{x}) \leqslant t\}. \qquad (2)$$

Its boundary, $\partial B(t; \mathbf{x}_0)$, will be termed the isochrone corresponding to time t. Balls and isochrones can be obtained using, e.g., Dijkstra's algorithm [29]. Throughout this work, all the balls will be centered at the origin of coordinates $\mathbf{x}_0 = \mathbf{0}$, so we will write simply $B(t)$.
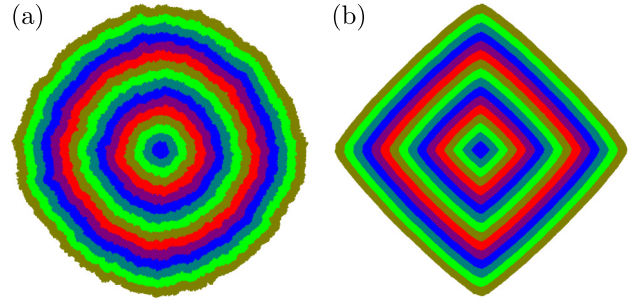

FIG. 1. Random balls $B(t)$ for an FPP system on a square lattice, centered on the origin of coordinates for different times. (a) Balls obtained for a uniform link-time distribution using $\mu = 5$ and CV = 0.57. (b) Balls obtained for a uniform link-time distribution using $\mu = 5$ and CV = 0.11. Colors are changed every $\Delta t = 100$, and the total lattice size is 500×500 for (a) and 250×250 for (b).

Following Ref. [17], we control the strength of the disorder through the coefficient of variation of the distribution, CV, defined as CV $= s/\mu$. It has been shown [18] that for strong disorder conditions (CV $\gg 1$), the isochrones grow initially as the clusters obtained in bond percolation with increasing occupation probability $p = F(t)$. Then a crossover takes place at a certain time, which increases monotonically with the disorder strength, from which the isochrones evolve towards the asymptotic circular shape with KPZ statistics. In this paper, we will focus on the dynamics and geometry of the isochrones in the weak disorder regime, i.e., when CV < 1 [17]. The CV has a strong effect on the shape of the isochrones, as illustrated in Fig. 1, where we can see circular isochrones associated to CV $= 0.57$, in Fig. 1(a), and diamondlike shapes associated to CV $= 0.11$, in Fig. 1(b).

To characterize the isochrones, we have performed numerical experiments on a $(2L + 1) \times (2L + 1)$ square lattice with $L = 1200$. In this paper, we will employ two different link-time distributions: First, a uniform distribution on an interval $[\tau_0, \tau_1]$, for which the maximal attainable value of CV is $1/\sqrt{3} \approx 0.58$, since $\tau_0 \geqslant 0$ necessarily. Furthermore, we have also employed a Weibull distribution, given by the probability density function

$$f(\tau) = \frac{k}{\lambda}\left(\frac{\tau}{\lambda}\right)^{k-1} \exp(-(\tau/\lambda)^k), \qquad (3)$$

with shape parameter $k > 1$, which is only defined for positive τ and allows any positive value for CV. Thus, we employ a bounded and an unbounded distribution—both of them fulfill the conditions for the limit shape theorem, i.e., all the moments exist and are finite, and $F(0) = 0$ [19,30].

In our simulations, we fix $\mu = 5$ and choose different values of CV in to survey the different possible limit shapes. Thus, we use the notations $U(\text{CV})$ and Wei(CV), respectively, for the uniform and Weibull distributions with parameter CV. In all simulations discussed in this paper, we employ $N_s = 10^4$ different noise realizations. Measurements are performed at $N_t = 100$ logarithmically distributed times, ranging from $t_{\min} = 10\mu = 50$ to $t_{\max}$, chosen so the average radius of the isochrone reaches $3L/4 = 900$.

III. SHAPE ANALYSIS

A. Limit shape and instantaneous average shape

The shape theorem ensures that the growth rates of the FPP isochrones along any fixed direction converge towards a limiting function, $v(\theta)$ [19,20,30]. In other terms, if we scale down the different isochrones, $t^{-1}\partial B(t)$, we will notice that, with probability one, they are contained in a deterministic, convex and compact set $\mathscr{B}$, which must be invariant under reflections around the axes of the underlying lattice. Under very general conditions, this limit shape is determined by $v(\theta)$. For large values of CV, this limit shape will be close to a circumference, while for small CV the average isochrone approaches a diamond shape [17], given by

$$\{(x, y) \in \mathbb{R}^2 \ : \ |x| + |y| = K\}, \tag{4}$$

where K is a constant ensuring that the average radius is 1:

$$K = \frac{\pi}{\sqrt{2}\log(2^{3/2}+3)} \approx 1.26. \tag{5}$$

Let us parametrize our isochrone as a polar curve for each time, $r(\theta, t)$. The mean circumference at time t will be centered at the origin, with radius given by

$$R(t) \equiv \overline{\langle r(\theta, t) \rangle}, \tag{6}$$

where we denote spatial averages over θ with an overbar, and averages over noise realizations with angular brackets. Let us then define an IAS as

$$R(\theta, t) \equiv \langle r(\theta, t) \rangle, \tag{7}$$

where the average is taken over all noise realizations. Note that this IAS need not coincide, in general, with the scaled version of the limit shape, $R(\theta, t) \neq t\, v(\theta)$. In fact, we can define a scaled IAS,

$$\rho(\theta, t) \equiv \frac{R(\theta, t)}{R(t)}, \tag{8}$$

that will approach the limit shape asymptotically,

$$\lim_{t \to \infty} \rho(\theta, t) = C\, v(\theta), \tag{9}$$

where C is a constant.

B. Characterization of the instantaneous average shape

We have evaluated the IAS $R(\theta, t)$ for different times and disorder distributions for the link times. For each noise realization and time, we obtain a discretized interface whose angular resolution $\Delta\theta$ decreases with time because the average radius grows with time. Indeed, we have determined our angular resolution dynamically by imposing that the number of points in each interval $\Delta\theta$ must remain between one and two throughout the simulation.

Figure 2 shows the scaled IAS, $\rho(\theta, t)$, for different times and disorder distributions as a function of the angle θ. Figure 2(a) shows the time evolution of the scaled IAS for the uniform link-time distributions using CV = 0.57 and CV = 0.11. Note that the scaled IAS converges very fast to a limit shape, as expected in Eq. (9). Figure 2(b) shows the limit shape obtained numerically for a variety of uniform and Weibull distributions. As a reference, we also show the
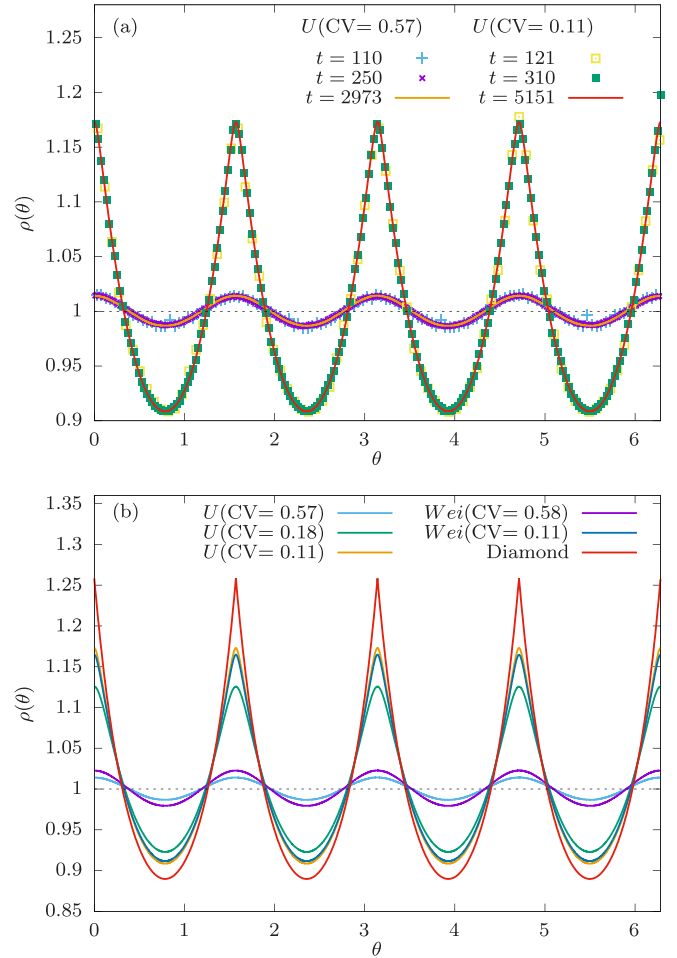

FIG. 2. (a) Time evolution of the scaled IAS, $\rho(\theta, t)$, for two uniform link-time distributions, using CV = 0.57 and CV = 0.11. (b) Limit shapes for different link-time distributions, all of them with expected value $\mu = 5$. The dashed line represents the circumference, and the perfect diamond shape, given by Eq. (4), is shown with a red continuous line with the maximal amplitude.

circumference, given by the horizontal dashed line, and the diamond, Eq. (4), shown as a red continuous line. We should stress that the mean value of the link-time distribution μ does not affect the limit shape.

We can express the scaled IAS at time t, $\rho(\theta, t)$, as a Fourier series:

$$\rho(\theta, t) = a_0 + \sum_{n=1}^{\infty} [a_n(t)\cos(n\theta) + b_n(t)\sin(n\theta)]. \tag{10}$$

Let us stress that $a_0 = 1$ in all cases for all times, and $b_n(t) = 0$ for all n due to reflection symmetry around each axis. Furthermore, $\pi/2$ rotational symmetry dictates that the only nonzero values for $a_n(t)$ are those with $n = 4k$ and $k \in \mathbb{N}$. Figure 3 shows the Fourier components for the limit shape, a_n, obtained for the uniform and Weibull link-time distributions using both CV = 0.57 (a) and CV = 0.11 (b). Note that for CV = 0.57 only a few a_n take nonzero values, while for CV = 0.11 we observe a behavior similar to the diamond shape, which is also shown for comparison. Figure 3 (insets) shows the time evolution of different Fourier components, $a_n(t)$,
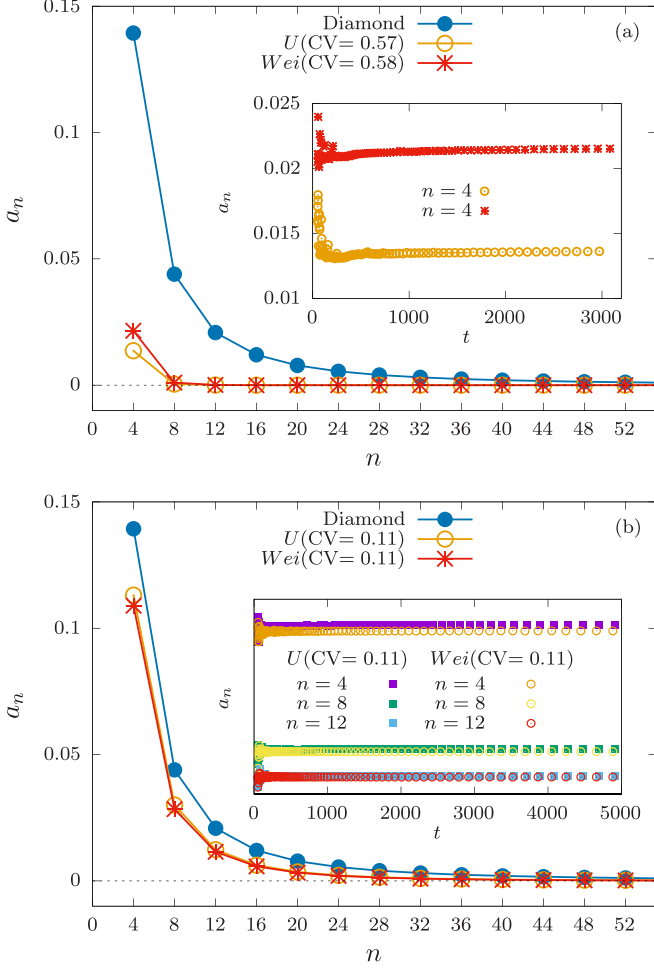
FIG. 3. Fourier decomposition of the limit shape, a_n, for the uniform and Weibull link-time distributions, with $\mu = 5$, employing CV = 0.57 in (a) and CV = 0.11 in (b). Insets: Time evolution of some selected Fourier coefficients of the scaled IAS, $a_n(t)$, using both CV = 0.57 and CV = 0.11 for the uniform and Weibull link-time distributions.

obtained for the uniform and Weibull link-time distribution using CV = 0.57 and CV = 0.11, where we can observe their fast convergence towards their limit shape values, that we will denote as a_n.

IV. ROUGHNESS AND CORRELATION LENGTH

A. Roughness

Let us now consider the roughness and the correlation lengths for the isochrones. In naive terms, we may define the isochrone roughness corresponding to time t as the deviation of all values $r(\theta, t)$ around their average value, $R(t)$ [9],

$$\sigma_r^2(t) \equiv \overline{\langle (r(\theta, t) - R(t))^2 \rangle}, \tag{11}$$

Indeed, this definition is not appropriate because the average shape is not circular. Thus, the roughness should be measured with respect to a suitable average shape. In fact, Fig. 4 shows the time evolution of this global roughness (solid lines), which grows with time as t^β with $\beta = 1$, very different from the expected $\beta = 1/3$ KPZ value [17]. The reason for this growth
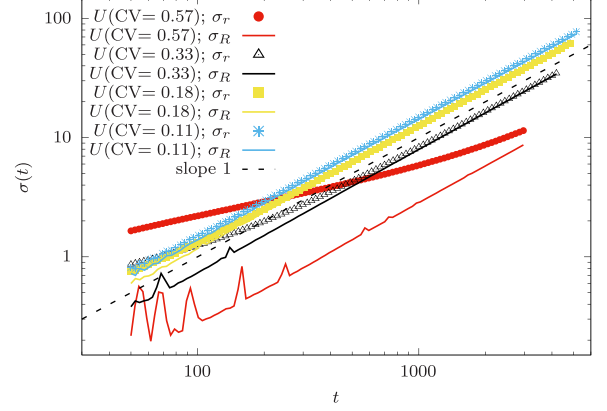

FIG. 4. Deviation of the interfacial radii of the isochrones, σ_r (symbols) and of the IAS radii, σ_R (solid lines) for several uniform distributions. The dashed line shows a power law behavior with exponent $\beta = 1$.

is that most of the radial deviation can be associated to the deviations of the IAS with respect to the mean circumference. Indeed, Fig. 4 shows also the deviation of the IAS radii, given by

$$\sigma_R^2(t) \equiv \overline{\langle (R(\theta, t) - R(t))^2 \rangle}, \tag{12}$$

which presents a similar scaling for small CV. Even for higher values of CV, we can observe that both deviations approach asymptotically for long times. Therefore, we can explain the $\beta = 1$ scaling: we are counting as roughness what is simply the form of the average isochrone, which is due to the lattice.

Let us provide the correct definition of the interface roughness, which is the root-mean-square deviation between the radii of the interfaces and the IAS:

$$W^2(t) \equiv \overline{\langle (r(\theta, t) - R(\theta, t))^2 \rangle}. \tag{13}$$

Figure 5 shows the time evolution of this roughness $W(t)$ for different noise distributions. As expected, this magnitude presents a scaling behavior associated to the KPZ universality class, $W(t) \sim t^\beta$ with $\beta = 1/3$ in all cases. We should remark that for higher values of CV, the exponent $1/3$ is rapidly attained, whereas the preasymptotic regime becomes longer for lower values of CV, as expected from previous works [17].
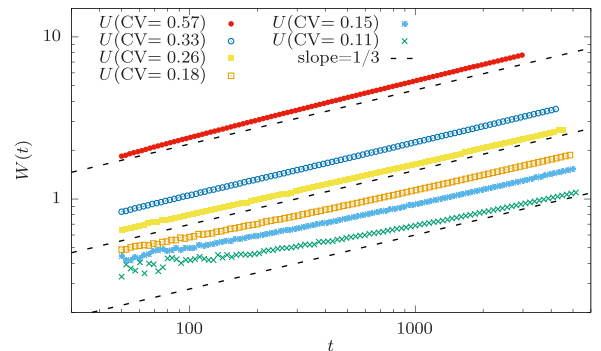

FIG. 5. Time evolution of the roughness $W(t)$, defined with respect to the IAS, as shown in Eq. (13), for uniform distributions. Dashed lines indicate power-law behavior with exponent $1/3$.
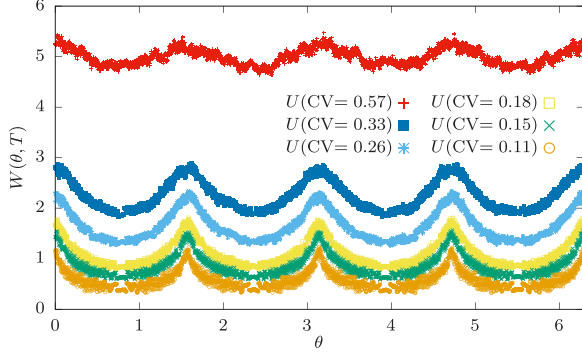
FIG. 6. Angular-resolved roughness, $W(\theta, t)$, for time t_{max}, using different uniform link-time distributions. Higher values of $W(\theta, T)$ correspond to higher values of CV.

FIG. 7. Growth of the correlation length for several uniform distributions. Dashed lines show a power-law behavior with exponent 2/3.

B. Angular-resolved roughness

Our definition of the roughness, given in Eq. (13), can be considered as an angular average of a certain angular-resolved roughness, which can be defined as

$$W^2(\theta, t) \equiv \langle (r(\theta, t) - R(\theta, t))^2 \rangle, \qquad (14)$$

such that

$$W(t) = \overline{W(\theta, t)}. \qquad (15)$$

Indeed, in Fig. 6 we can observe the angular-resolved roughness $W(\theta, t)$ obtained at time t_{max} using several uniform link-time distributions. We note that this roughness presents a strong anisotropy for small values of CV, as expected. Indeed, the roughness is always larger near the lattice axes.

C. Correlation length

On the other hand, the scaling of the correlation length with time allows us to obtain the dynamic exponent z from the evolution of the correlation length, $\xi \sim t^{1/z}$. We will estimate its value using the technique developed in Ref. [6], which is based on the notion of patches. A patch is defined as a section of the isochrone such that all its points are either above or below the IAS. The patch length is then defined as the projection of this subset of the isochrone onto the average circumference. Let n be the number of patches of a given isochrone, whose lengths are given by $\{\ell_i\}_{i=1}^n$. To estimate the correlation length, we randomly choose a point over the average shape and find the expected value of the length of its associated patch. In other words, we select patch i with probability $\ell_i / \sum_i \ell_i$, and we can estimate

$$\xi \equiv \left\langle \frac{\sum_i \ell_i^2}{\sum_i \ell_i} \right\rangle, \qquad (16)$$

which is expected to grow as $\xi(t) \sim t^{1/z}$.

We have evaluated the behavior of $\xi(t)$ for all the considered distributions of disorder, and the results for several uniform distributions are displayed in Fig. 7. We obtain, in all cases, a power law with an exponent very close to 2/3. These results are in agreement with a value for the dynamic exponent of $z = 3/2$, associated to the KPZ universality class.
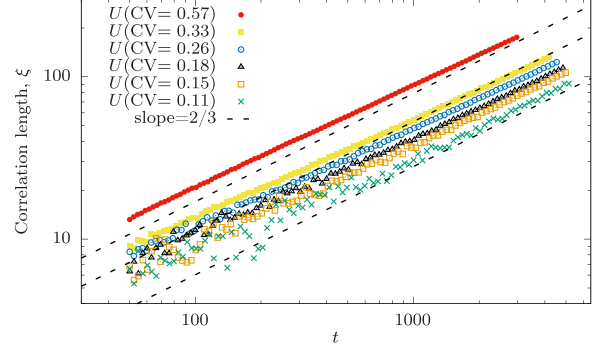
V. RADIAL FLUCTUATIONS

As discussed in the Introduction, the height fluctuations in 1+1D KPZ systems follow the TW probability distribution [14], which somehow plays a similar role to that of the Gaussian distribution in the central limit theorem. The TW distribution comes in different flavors and the Gaussian orthogonal ensemble (TW-GOE) is typically associated to flat interfaces, while the Gaussian unitary ensemble (TW-GUE) is typically connected to circular interfaces.

In a model with rotational symmetry, we can consider all the radii of the different interfaces, labeled by their time, $\{r_i(t)\}$. Then, we fit the average radius as a function of time to a form $\langle r_i(t) \rangle \approx r_0 + vt$, choosing the best possible values of r_0 and v. Then we fit the time dependence of their deviations to a form $\sigma[r_i(t)] \approx \Gamma t^\beta$. Finally, we define a random variable χ_i implicitly through the expression

$$r_i = r_0 + vt + \Gamma t^\beta \chi_i. \qquad (17)$$

If the interface follows KPZ scaling, we expect the random variable χ to present a stationary probability distribution that will approach the TW-GUE distribution, rescaled to have zero average and unit deviation [5,6].

The same TW-GUE distribution has been found in FPP models, for example, in the times of arrival along the axis and diagonal directions [17]. Yet, KPZ scaling suggests that it should also determine the radial fluctuations of the isochrones, and in this section we will show that this is indeed the case, provided that these radial fluctuations are appropriately scaled.

Let us choose a point $\mathbf{x_i} = (r_i, \theta_i)$ along the interface and let $R(\theta, t)$ be the radius of the IAS along the same direction for that time. Then, we can define

$$r = R(\theta, t) + \Gamma(\theta) t^{1/3} \chi, \qquad (18)$$

where χ should be a stationary random variable following the (rescaled) TW-GUE distribution and $\Gamma(\theta)$ is chosen so the angular-resolved roughness, defined in Eq. (14), behaves as

$$W(\theta, t) \approx \Gamma(\theta) t^\beta. \qquad (19)$$

Thus, in our case, we must employ two labels for the radial data, i.e., the time and the angle θ.

Numerically, we proceed as follows. We select a certain angular width $\Delta\theta \approx 10^{-3}$ and bin our radial data according
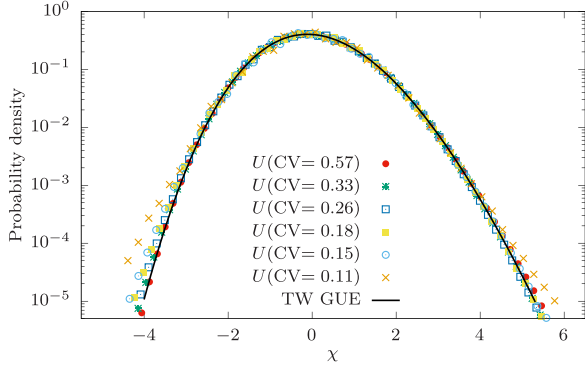
FIG. 8. Histograms for the rescaled radial fluctuations, following Eq. (18) for several uniform distributions.

to time and angle. For each bin, we subtract the expected average, which corresponds to the radius of the IAS, and divide by their deviation, which corresponds to the associated angular-resolved roughness:

$$\chi_i = \frac{r_i - R(\theta, t)}{W(\theta, t)}. \tag{20}$$

We then obtain the histograms for these values in Fig. 8, which corresponds to the TW-GUE distribution as expected. The histograms are computed using all available times for which the condition $W(t) \sim t^\beta$ holds.

Figure 9 shows the histograms for the radial fluctuations, $r(\theta, T) - R(\theta, T)$, without rescaling with the corresponding deviation, along the axis and diagonal directions for different values of CV. The measurement time is $t_{\max}$, and to obtain enough data we employ angular windows of width $\Theta = 1/3$ radians along both directions. Figure 9(a) shows the histograms for CV = 0.57, and we can see that the distributions for both directions are rather similar, both corresponding to the TW-GUE distribution as expected. The inset panel shows how they coincide when the fluctuations are rescaled to have unit variance. Figure 9(b), on the other hand, shows the histograms for CV = 0.11, where we can observe that the fluctuations along the axis and the diagonal directions are very different, while they coincide when correctly rescaled, as shown in the inset. A naive averaging of the fluctuations along different directions, without proper rescaling with the appropriate deviations, would lead to an average histogram which departs enormously from the TW-GUE distribution, showing indeed a large value for the kurtosis.

VI. MORPHOLOGICAL ANALYSIS

Let us consider the roughness exponent, α, which characterizes the stationary regime attained when the correlation length reaches the system size L. According to the Family-Vicsek dynamic scaling ansatz [9], we have

$$W(L, t) = t^\beta \, g(L/t^{1/z}), \tag{21}$$

where the scaling function $g(u)$ has the general form

$$g(u) = \begin{cases} \text{const.} & \text{if } u \gg 1 \\ u^\alpha & \text{if } u \ll 1. \end{cases} \tag{22}$$
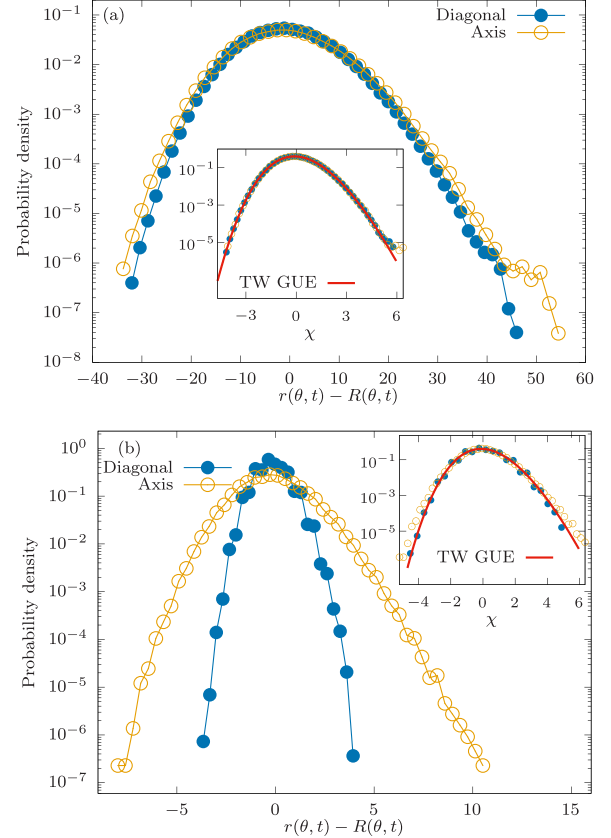

FIG. 9. Histogram of the radial fluctuations, $r(\theta, t) - R(\theta, t)$, without proper rescaling with the deviation, performed for the axial and diagonal directions with an angular window of $\Theta = 1/3$ radians, using (a) $U(\text{CV} = 0.57)$ and (b) $U(\text{CV} = 0.11)$ for time $t_{\max}$. Insets: Histograms of the rescaled radial fluctuations for the same directions.

This expression cannot be applied to radially growing systems in which the system size increases linearly with time because in those cases the stationary regime is never attained [31–33]. Yet, the power-law behaviors of the roughness $W(t) \sim t^\beta$ and the correlation length $\xi(t) \sim t^{1/z}$, along with the Galilean scaling relation for KPZ, $\alpha + z = 2$, all suggest $\alpha = 1/2$ for our system, but we should check this value independently.

To characterize the morphological properties of the isochrones, we define the scale-resolved roughness, $w(l, t)$, as the average roughness for windows of size l measured on the average circumference of radius $R(t)$ [34,35],

$$w^2(l, t) \equiv \langle [(r(\theta, t) - R(t))^2]_l \rangle, \tag{23}$$

where $[\cdots]_l$ denotes the average over linear windows of size l, whose location does not depend on θ. We expect the following scaling ansatz, similar to Eq. (22):

$$w(l, t) = t^\beta g_{\text{loc}}(l/t^{1/z}), \tag{24}$$

where now $g_{\text{loc}}(u)$ behaves as u^{α_l} if $u \ll 1$ and as a constant for $u \gg 1$, where α_l is termed the local roughness exponent. Thus, for a fixed value l we expect the local roughness to grow as t^β up to a saturation time, when the correlation length reaches l. From this moment on, the window roughness saturates at a value that scales as l^{α_l}.
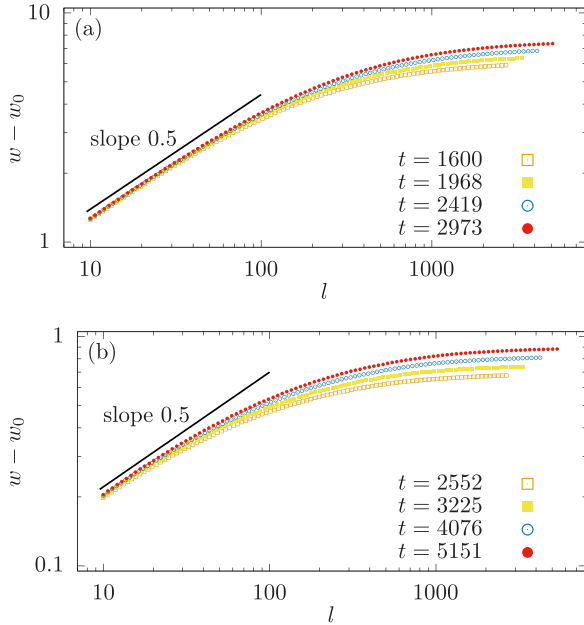
FIG. 10. Scale-resolved roughness, subtracting the intrinsic roughness, $w(l, t) - w_0$, as a function of l for disorder distributions $U(\mathrm{CV} = 0.57)$ (a) and $U(\mathrm{CV} = 0.11)$ (b).

We should adapt our measurements of the local roughness, Eq. (23), to our anisotropic case:

$$w(l, t) = \langle [(r(\theta, t) - R(\theta, t))^2]_l \rangle. \tag{25}$$

The results of our numerical simulations are shown in Fig. 10, where the scale-resolved roughness is plotted for different times, using uniform link distributions with CV = 0.57 and CV = 0.11. The proper small-length scaling is obtained assuming that the system presents certain intrinsic roughness,

$$w(l, t) \approx w_0 + A l^\alpha, \tag{26}$$

where $\alpha = 1/2$ in all cases, $w_0 \approx 0.17$ for CV = 0.57, and $w_0 \approx 0.2$ for CV = 0.11. This intrinsic roughness can mask the correct scaling if it is not properly taken into account. We conjecture that its physical origin is related to the uncertainty in the measurement of the IAS.

VII. CONCLUSIONS AND FURTHER WORK

In this paper, we have characterized the statistical properties of the isochrones of the FPP problem on a square lattice, showing that they correspond to the KPZ universality class. The main difficulty lies in the fact that the average isochrone deviates substantially from the circumference when the CV is small, due to the strong anisotropy of the system. To reveal the hidden KPZ scaling, we have defined the IAS for each noise

level and time, and characterized them using their Fourier representation. Indeed, for CV ≈ 1 they approach a circumference, while for CV $\ll 1$ they approach a diamond. We also define an angular-resolved roughness, which depends on the direction of growth, showing a similar behavior. Indeed, the fluctuations are always higher along the axis than along the diagonal, with the anisotropy again growing for lower values of CV.

Once the radial fluctuations are measured with respect to the IAS and their deviations are scaled with an angular-dependent factor, all the hallmarks of the 1+1D KPZ class appear clearly: the roughness grows as $W(t) \sim t^\beta$ with the growth exponent $\beta = 1/3$, and the correlation length grows as $\xi(t) \sim t^{1/z}$ with the dynamic exponent $z = 3/2$. Moreover, if the radial fluctuations are scaled with an angular-dependent factor, they are shown to follow the expected TW-GUE distribution. The local roughness can be shown to scale as $w(l) \sim l^{\alpha_l}$ for $l \ll \xi(t)$, with $\alpha_l = 1/2$, if we subtract previously an intrinsic roughness w_0 which depends weakly on the link-time distribution, and which is probably related to the uncertainty in our estimation of the IAS.

Our procedure to subtract the IAS will be of interest to analyze other systems, both continuous or discrete, which present noncircular characteristic shapes around which the fluctuations should be measured. The first such application should be to growing interfaces defined on a lattice, when the lattice effects are suspected to spoil the scaling analysis and the characterization of the universality class [24,25,36]. Physically, lattice effects may be induced by, e.g., crystallographic directions, as in epitaxial growth of thin solid films [22,23]. Furthermore, the subtraction of the average shape can be useful in cases of morphopological instabilities, where a nontrivial average shape can be established at short times, which may, in turn, have an effect in the determination of the universal properties of the fluctuations [37,38].

[1] R. Adler and J. Taylor, *Random Fields and Geometry* (Springer, Berlin, 2007).

[2] T. Halpin-Healy and Y.-C. Zhang, Phys. Rep. **254**, 215 (1995).

[3] J. Ambjørn, B. Durhuus, and T. Jonsson, *Quantum Geometry: A Statistical Field Theory Approach* (Cambridge University Press, Cambridge, 1997).

[4] D. Nelson, T. Piran, and S. Weinberg, *Statistical Mechanics of Membranes and Surfaces* (World Scientific, Singapore, 2004).

[5] S. N. Santalla, J. Rodriguez-Laguna, T. LaGatta, and R. Cuerno, New J. Phys. **17**, 033018 (2015).

[6] S. N. Santalla, J. Rodriguez-Laguna, A. Celi, and R. Cuerno, J. Stat. Mech. (2017) 023201.

[7] M. Kardar, G. Parisi, and Y.-C. Zhang, Phys. Rev. Lett. **56**, 889 (1986).

[8] M. Kardar and Y.-C. Zhang, Phys. Rev. Lett. **58**, 2087 (1987).

[9] A.-L. Barabási and H. E. Stanley, *Fractal Concepts in Surface Growth* (Cambridge University Press, Cambridge, 1995).

[10] J. M. Hammersley and D. J. A. Welsh, First-passage percolation, subadditive processes, stochastic networks and generalized renewal theory, in *Bernoulli, Bayes, Laplace Anniversary Volume*, edited by J. Neyman and L. M. LeCam (Springer, Berlin, 1965).

[11] J. F. C. Kingman, J. R. Stat. Soc. B **30**, 499 (1968).

[12] D. Romik, *The Surprising Mathematics of Longest Increasing Subsequences* (Cambridge University Press, Cambridge, 2015).

[13] M. Prähofer and H. Spohn, J. Stat. Phys. **108**, 1071 (2002).

[14] K. A. Takeuchi, M. Sano, T. Sasamoto, and H. Spohn, Sci. Rep. **1**, 34 (2011).

[15] I. Corwin, J. Quastel, and D. Ramenik, Commun. Math. Phys. **317**, 347 (2013).

[16] M. L. Mehta, *Random Matrices* (Elsevier, Amsterdam, 2004).

[17] P. Córdoba-Torres, S. N. Santalla, J. Rodríguez-Laguna, and R. Cuerno, J. Stat. Mech. (2018) 063212.

[18] D. Villarrubia, I. Álvarez Domenech, S. N. Santalla, J. Rodríguez-Laguna, and P. Córdoba-Torres, Phys. Rev. E **101**, 062124 (2020).

[19] J. T. Cox and R. Durrett, Ann. Probab. **9**, 583 (1981).

[20] M. Damron, Random growth models shape and convergence rate, in *Random Growth Models*, edited by M. Damron, F. Rassoul-Agha, and T Seppäläinen (AMS Joint Mathematics Meetings, Atlanta, 2017).

[21] R. Savit and R. Ziff, Phys. Rev. Lett. **55**, 2515 (1985).

[22] P. Jensen, Rev. Mod. Phys. **71**, 1695 (1999).

[23] C. Misbah, O. Pierre-Louis, and Y. Saito, Rev. Mod. Phys. **82**, 981 (2010).

[24] D. Bonn, J. Eggers, J. Indekeu, J. Meunier, and E. Rolley, Rev. Mod. Phys. **81**, 739 (2009).

[25] J. M. Marcos, P. Rodríguez-López, J. J. Meléndez, R. Cuerno, and J. J. Ruiz-Lorenzo, Phys. Rev. E **105**, 054801 (2022).

[26] Y. Chen, E. López, S. Havlin, and H. E. Stanley, Phys. Rev. Lett. **96**, 068702 (2006).

[27] S. V. Buldyrev, S. Havlin, and H. E. Stanley, Phys. Rev. E **73**, 036128 (2006).

[28] A. Hansen and J. Kertész, Phys. Rev. Lett. **93**, 040601 (2004).

[29] T. H. Cormen, C. E. Leiserson, R. L. Rivest, and C. Stein, *Introduction to Algorithms* (The MIT Press, Cambridge, 1990).

[30] H. Kesten, Aspects of first passage percolation, in *École d'Été de Probabilités de Saint Flour XIV- 1984*, edited by P. L. Hennequin (Springer, Berlin, Heidelberg, 1986).

[31] A. Brú, S. Albertos, J. L. Subiza, J. L. García-Asenjo, and I. Brú, Biophys. J. **85**, 2948 (2003).

[32] S. N. Santalla, J. Rodríguez-Laguna, and R. Cuerno, Phys. Rev. E **89**, 010401(R) (2014).

[33] J. Galeano, J. Buceta, K. Juarez, B. Pumariño, J. de la Torre, and J. M. Iriondo, Europhys. Lett. **63**, 83 (2003).

[34] J. J. Ramasco, J. M. López, and M. A. Rodríguez, Phys. Rev. Lett. **84**, 2199 (2000).

[35] J. M. López, M. A. Rodríguez, and R. Cuerno, Physica A **246**, 329 (1997).

[36] S. C. Ferreira Jr. and S. G. Alves, J. Stat. Mech. (2006) P11007.

[37] M. Castro, R. Cuerno, M. Nicoli, L. Vázquez, and J. G. Buijnsters, New J. Phys. **14**, 103039 (2012).

[38] S. N. Santalla, J. Rodríguez-Laguna, J. P. Abad, I. Marín, M. M. Espinosa, J. Muñoz-García, L. Vazquez, and R. Cuerno, Phys. Rev. E **98**, 012407 (2018).